Phonon dispersion and lifetimes in MgB2.

Phonon Dispersion and Lifetimes in MgB_2

Abhay Shukla,[1] Matteo Calandra,[1] Matteo d'Astuto,[2] Michele Lazzeri,[1] Francesco Mauri,[1] Christophe Bellin,[1] Michael Krisch,[2] J. Karpinski,[3] S. M. Kazakov,[3] J. Jun,[3] D. Daghero,[4] and K. Parlinski[5]

[1]*Laboratoire de Minéralogie-Cristallographie, case 115, 4 Place Jussieu, 75252, Paris cedex 05, France*
[2]*European Synchrotron Radiation Facility, BP 220, F-38043 Grenoble cedex, France*
[3]*Solid State Physics Laboratory, ETH, CH-8093 Zürich, Switzerland*
[4]*INFM, Dipartimento di Fisica, Politecnico di Torino, C. Duca degli Abruzzi 24, 10129 Torino, Italy*
[5]*Institute of Nuclear Physics, ulica Radzikowskiego, 152, 31-342, Cracow, Poland*

(Received 3 September 2002; published 7 March 2003)

We measure phonon dispersion and linewidth in a single crystal of MgB_2 along the Γ-A, Γ-M, and A-L directions using inelastic x-ray scattering. We use density functional theory to compute the effect of both electron-phonon coupling and anharmonicity on the linewidth, obtaining excellent agreement with experiment. Anomalous broadening of the E_{2g} phonon mode is found all along Γ-A. The dominant contribution to the linewidth is always the electron-phonon coupling.

DOI: 10.1103/PhysRevLett.90.095506 PACS numbers: 63.20.Dj, 63.20.Kr, 71.15.Mb, 78.70.Ck

The discovery of 39 K superconductivity in MgB_2 [1] has led to in-depth study of the material and a picture has emerged of a phonon-mediated superconductor with multiple gaps [2–4], moderate electron-phonon coupling (EPC) [3,5–7], and anharmonicity [3,4,8–10]. However, no measurements exist concerning either phonon dispersion or the evolution of phonon lifetimes over the Brillouin zone (BZ), due to the absence of large single crystals. Neutron scattering on powder samples [8,11] has been limited to the determination of phonon density of states. Raman spectroscopy, which is restricted to the BZ center, has shown that the optical mode with E_{2g} symmetry, corresponding to in-plane distortions of the B hexagons, is strongly damped [12–15].

Phonon damping can be caused by (i) EPC mediated phonon decay into electron-hole pairs [16] or (ii) phonon-phonon interaction due to anharmonicity [17]. The linewidth (the inverse of the lifetime) of a given phonon is the sum of both contributions. Direct determination of the contribution of each phonon mode to EPC [16] from the measured linewidth is possible only if the anharmonic contribution is negligible [18] and is seemingly questionable for MgB_2 where many calculations [3,4,8] suggest strong anharmonic effects.

In this work we present the first measured phonon dispersion curves and linewidths (where possible) along three directions in the BZ, Γ-A, Γ-M, and A-L. We circumvented the problem of sample size by using high-resolution inelastic scattering of a focused and intense x-ray beam at the European Synchrotron Radiation Facility (beam line ID28), a technique [19] successfully used in single crystalline samples and, in particular, for the measurement of high energy optical modes [20]. To understand the mechanisms governing the measured phenomena, we calculated phonon dispersion, the contributions of EPC and anharmonicity to the linewidth, and the structure factors using density functional theory (DFT).

Small single crystals of MgB_2, suitable for inelastic x-ray scattering experiments, have recently become available. The crystal used in our experiment was grown at a pressure of 30–35 kbar. A mixture of Mg and B was put into a boron nitride container in a cubic anvil device. The temperature was increased during 1 h up to 1700–1800 °C, kept stable for 1–3 h, and decreased during 1–2 h. As a result, platelike MgB_2 crystals were formed of which we used a sample of about $400 \times 470 \times 40\ \mu m^3$, with a measured in-plane mosaicity of 0.007°. The beam incident on the sample was obtained from a high-resolution silicon backscattering monochromator using the (8 8 8) reflection at an incident energy of 15.816 keV. The x-ray beam was focused onto the sample by a toroidal mirror into a spot of $270 \times 90\ \mu m^2$ (horizontal $\times$ vertical), full width at half maximum (FWHM). Slits before the sample further limited the vertical beam size to 30 μm. The scattered photons were analyzed in energy by five spherical silicon crystal analyzers operating at the same reflection order and mounted in pseudo Rowland circle geometry. The total energy resolution was 6.1 meV FWHM, as determined by a fit to a Lorentzian line shape. The momentum transfer $\mathbf{Q}$ was selected by rotating the 7 m long analyzer arm around the sample position, in the horizontal plane, which also contained the linear x-ray polarization vector of the incident beam. The momentum resolution was set to 0.04 $Å^{-1}$ in the horizontal direction and 0.07 $Å^{-1}$ in the vertical direction. The following measurements were performed at a temperature of 300 K: (i) $\mathbf{Q} = (1\ 2\ \xi)$, in almost transverse configuration along the Γ-A direction, i.e., with $\mathbf{Q} \cdot q \approx 0$, $\mathbf{q} = (0\ 0\ \xi)$ being the phonon wave vector; (ii) $\mathbf{Q} = (1-\delta\ 1+\xi\ 0)$, while nearly following the Γ-M direction ($0 \leq \delta \leq 0.05$); (iii) $\mathbf{Q} = (1-\delta_1\ 2+\xi\ 0.5+\delta_2)$, while nearly following the A-L direction ($0 \leq \delta_1, \delta_2 \leq 0.04$). The choice of BZ points measured was dependent on a series of conditions

including the need to optimize the structure factors, single (Γ-A) or multianalyzer (Γ-M, A-L) measurement mode, and spectrometer and time limitations.

In Fig. 1 we show data taken at the 0.6 Γ-A point in the BZ. The acoustic mode as well as the lower energy optical mode (E_{1u}) are visible as resolution-limited peaks. Most importantly, a broad peak is observed at higher energy loss, corresponding to the E_{2g} mode. We performed least square fits to sums of Lorentzian functions with FWHM corresponding to the experimental resolution for the resolution-limited peaks and a free parameter for the strongly damped phonon. These yield the dispersion as well as the linewidth variation over the BZ. Despite statistical limitations (3–6 counts/min on this peak along Γ-A) and tails of the peaks from the stronger, low energy phonons, the peak energy as well as the linewidth can be estimated with reasonable confidence.

Figure 2 shows a similar energy loss scan at (0.97 2.29 0.54) close to the 0.58 A-L point. A strong acoustic mode is seen at 30 meV. The peak at 50 meV corresponds to the A_{2u} branch and the one at 65 meV to another acoustic branch. Finally, two resolved features are seen at 85 and 97 meV. These are the two E_{2g} modes which in this region of reciprocal space are well separated from other modes. Though, given the statistics, it would be hazardous to estimate a linewidth, the comparison between the experimental and *ab initio* spectra suggests that the linewidths of both the E_{2g} modes are resolution limited and so the damping is much less than that along Γ-A. As for the measurement nearly along Γ-M, the structure factor for the optical modes strengthens only near the zone boundary. At the point measured nearest to M [(1.05 1.45 0), not shown], the E_{2g} and E_{1u} modes are comparable in intensity but separated by only about 1 meV according to our calculation and we do measure a single peak only somewhat broader (FWHM $\approx$ 10 meV) than the experimental resolution, indicating reduced E_{2g} linewidth. The proximity of the E_{1u} mode, however, prevents a firm conclusion in this regard. We mention that the calculated structure factors and energies show excellent quantitative agreement with our measured data of which we have shown only two examples.

Similar analysis was done for several points along the three directions in order to experimentally determine the phonon dispersion and the linewidths. The difference in calculated phonon energies between the measured points and corresponding points exactly along Γ-M and A-L (δ, δ_1, $\delta_2 = 0$) is less than half a meV in all cases. We can thus compare the experimental phonon dispersion with the theoretical calculation along the high-symmetry lines, as shown in the bottom panel in Fig. 3 (circles).

The measured intrinsic linewidth of the E_{2g} branch, shown in the top panel in Fig. 3, is strongly anisotropic in the BZ. Along Γ-A it is particularly large (ranging from 20 to 28 meV), while near L and probably near M it is below the experimental resolution.

Electronic structure calculations [21] were performed using DFT in the generalized gradient approximation [22]. We used norm conserving pseudopotentials [23]. For Mg we used nonlinear core corrections [24] and we treated the $2s$, $2p$ levels as core states. The wave functions were expanded in-plane waves using a 35 Ry cutoff. The calculations were performed with the experimental crystal structure, namely, $a = 3.083$ Å and $c/a = 1.142$.

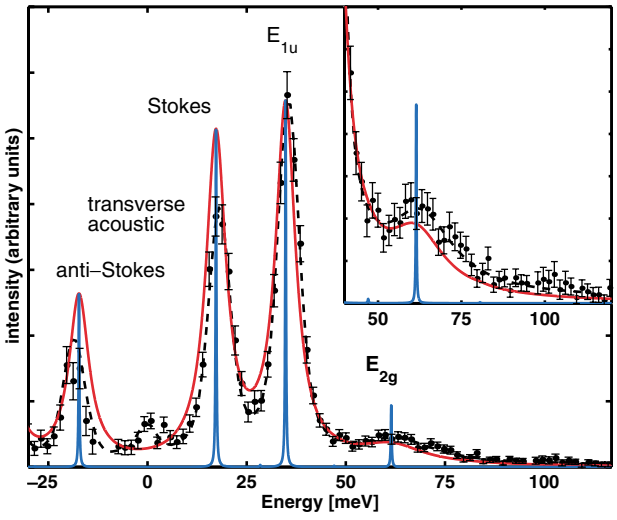

FIG. 1 (color online). Energy loss scan in almost transverse geometry measured at $\mathbf{Q} = (1\ 2\ 0.3)$ corresponding to 0.6 Γ-A. The data, normalized to the incident flux, are shown with the least-squares fit (dashed line) and the *ab initio* spectrum with and without broadening due to experiment and electron phonon coupling (solid lines). The broad peak corresponds to the damped E_{2g} mode and is shown in greater detail in the inset. The peak at zero is due to diffuse scattering.

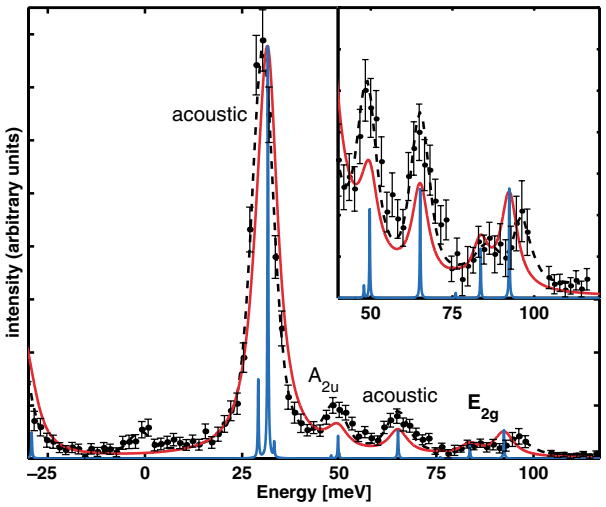

FIG. 2 (color online). Energy loss scan, measured at $\mathbf{Q} = (0.97\ 2.29\ 0.54)$ corresponding closely to 0.58 A-L, with the least-squares fit and the *ab initio* spectrum calculated at 0.58 A-L.

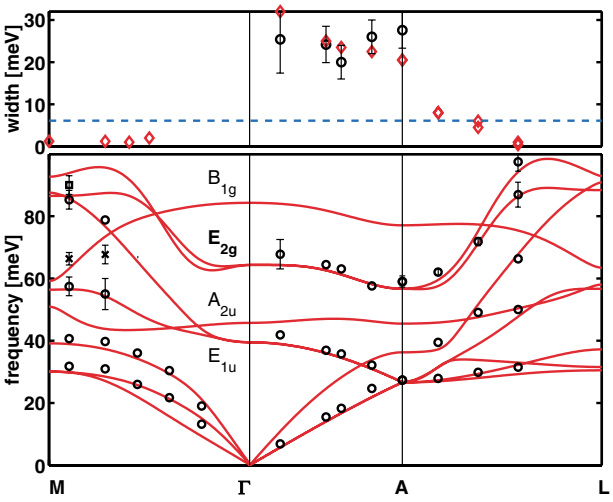

FIG. 3 (color online). Bottom: Experimental (circles) and theoretical phonon dispersion (solid line) in MgB_2 along Γ-A, Γ-M, and A-L. In the region near the M point, the probable detection of the E_{2g} mode is indicated with a square symbol (see text). The crosses indicate a parasite signal of unknown origin. Top: Intrinsic linewidth of the E_{2g} mode. The experimental linewidth (circles) is large along Γ-A and below the experimental resolution (dashed line) near L and M. The theoretical result (diamonds) for the electron-phonon coupling contribution to the linewidth is also shown. Along A-L and Γ-M where the E_{2g} mode is nondegenerate, both theoretical values are shown, when different. E_{2g} linewidth decreases progressively from A to L and experimentally the two branches are resolved for the point nearest to L.

The harmonic phonon frequencies were computed in the linear response [25]. We used a $16 \times 16 \times 16$ Monkhorst-Pack grid for the electronic BZ integration and first order Hermite-Gaussian smearing [26] of 0.025 Ry. The dynamical matrix at a given point of the BZ was obtained from a Fourier interpolation of the dynamical matrices computed on a $6 \times 6 \times 4$ phonon mesh. The resulting phonon frequencies are shown in Fig. 3 and are in good agreement with a recent calculation [12]. The agreement with experiment is remarkable.

The contribution to the FWHM linewidth $\gamma_{\mathbf{q}\nu}$ at momentum $\mathbf{q}$ for the ν phonon mode due to the electron-phonon interaction can be written as [16]:

$$\gamma_{\mathbf{q}\nu} = \frac{4\pi\omega_{\mathbf{q}}}{N_k} \sum_{\mathbf{k},n,m} |g^{\nu}_{\mathbf{k}n,\mathbf{k}+\mathbf{q}m}|^2 \delta(\varepsilon_{\mathbf{k}n}) \delta(\varepsilon_{\mathbf{k}+\mathbf{q}m}), \qquad (1)$$

where the sum is extended over the BZ, N_k is the number of k points in the sum, and $\varepsilon_{\mathbf{k}n}$ are the energy bands measured with respect to the Fermi level at point $\mathbf{k}$. The matrix element is $g^{\nu}_{\mathbf{k}n,\mathbf{k}+\mathbf{q}m} = \langle \mathbf{k}n | \delta V / \delta u_{\mathbf{q}\nu} | \mathbf{k}+\mathbf{q}m \rangle / \sqrt{2\omega_{\mathbf{q}\nu}}$, where $u_{\mathbf{q}\nu}$ is the amplitude of the displacement of the phonon ν of wave vector $\mathbf{q}$, $\omega_{\mathbf{q}\nu}$ is the phonon frequency, and V is the Kohn-Sham potential.

In the calculations we used $N_k = 30^3$ inequivalent k points, obtained from a mesh randomly shifted from Γ, and in Eqs. (1) and (3) we substituted the δ functions with Gaussians. The electron-phonon coupling $\lambda_{\mathbf{q}\nu}$ is obtained from the linewidth [16] as:

$$\lambda_{\mathbf{q}\nu} = \frac{\gamma_{\mathbf{q}\nu}}{2\pi N(0)\omega^2_{\mathbf{q}\nu}}, \qquad (2)$$

$N(0) = 0.354$ states/(MgB_2 eV spin) being the density of states at the Fermi level.

The second contribution to the linewidth is given by the anharmonicity in the crystal potential. At lowest order for the mode ν of a zone center phonon the FWHM linewidth is [17,27,28]:

$$\Gamma_{\mathbf{0}\nu} = \frac{\pi\hbar}{8N_q} \sum_{\mathbf{q},\mu\eta} \left| \frac{\partial^3 E}{\partial u_{\mathbf{0}\nu} \partial u_{\mathbf{q}\mu} \partial u_{-\mathbf{q}\eta}} \right|^2 \frac{I^{\mathrm{D}}_{\mathbf{q}\mu\eta\nu} + I^{\mathrm{A}}_{\mathbf{q}\mu\eta\nu}}{\omega_{\mathbf{0}\nu}\omega_{\mathbf{q}\mu}\omega_{\mathbf{q}\eta}}, \qquad (3)$$

E being the energy per cell, $n_{\mathbf{q}\mu}$ the Bose occupation for mode μ at wave vector $\mathbf{q}$, $I^{\mathrm{D}}_{\mathbf{q}\mu\eta\nu} = (n_{\mathbf{q}\mu} + n_{\mathbf{q}\eta} + 1) \times \delta(\omega_{\mathbf{0}\nu} - \omega_{\mathbf{q}\mu} - \omega_{\mathbf{q}\eta})$ describes the decay in the two phonons μ and η, and $I^{\mathrm{A}}_{\mathbf{q}\mu\eta\nu} = 2(n_{\mathbf{q}\mu} - n_{\mathbf{q}\eta}) \times \delta(\omega_{\mathbf{0}\nu} - \omega_{\mathbf{q}\mu} + \omega_{\mathbf{q}\eta})$ describes the η-phonon absorption and the μ-phonon emission.

We computed the anharmonic linewidth at the high-symmetry points Γ, A, and M. For the calculation at A we consider a $1 \times 1 \times 2$ supercell with 6 atoms, while for the M point we use a $2 \times 2 \times 1$ cell with 12 atoms. The third order matrices were evaluated using linear response theory and the $2n + 1$ theorem for metals [29]. The anharmonic contribution was evaluated at 0 and 300 K.

At Γ the anharmonic linewidth is largest for the E_{2g} mode and equal to 0.16 meV at $T = 0$ K and 1.21 meV at $T = 300$ K. Both the values are negligible if compared with the experimental Raman linewidth of roughly 40 meV [14], suggesting that the main source of broadening is the electron-phonon interaction.

The results of the calculation of the two contributions to the linewidth at A and M are shown in Table I. At the A

TABLE I. Calculated linewidths (meV) due to anharmonicity at 0 K (Γ^0_ν), 300 K (Γ^{300}_ν), and electron-phonon interaction γ_ν at M and A for all modes. Phonon frequencies increase from top to bottom. λ_ν is the electron-phonon coupling. E_{2g} modes are in boldface.

M				A			
Γ^0_ν	Γ^{300}_ν	γ_ν	λ_ν	Γ^0_ν	Γ^{300}_ν	γ_ν	λ_ν
0.00	0.12	0.00	0.00	0.00	0.17	0.00	0.00
0.00	0.15	0.01	0.01	0.00	0.17	0.00	0.00
0.02	0.12	0.06	0.02	0.00	0.63	0.08	0.05
0.12	0.48	1.13	0.20	0.00	0.63	0.08	0.05
0.06	0.25	0.00	0.00	0.02	0.22	0.84	0.28
0.07	0.33	2.34	0.30	0.02	0.20	0.08	0.02
0.26	**0.42**	**1.06**	**0.06**	**0.10**	**2.13**	**20.35**	**2.83**
0.45	0.69	1.21	0.07	**0.10**	**2.13**	**20.35**	**2.83**
0.47	**0.72**	**0.08**	**0.00**	0.13	0.23	0.05	0.00

TABLE II. Experimental and theoretical $\lambda_{\mathbf{q}\nu}$ of each of the two degenerate E_{2g} modes along Γ-A.

$\mathbf{q}$	0.2 Γ-A	0.5 Γ-A	0.6 Γ-A	0.8 Γ-A	1.0 Γ-A
$\lambda_{\mathbf{q}\nu}^{\text{expt.}}$	2.5 ± 1.1	2.6 ± 0.6	2.3 ± 0.5	3.6 ± 0.7	3.6 ± 0.8
$\lambda_{\mathbf{q}\nu}^{\text{theo.}}$	3.32	2.80	2.77	3.12	2.83

point the linewidth of the E_{2g} mode due to electron-phonon scattering is very large, while the anharmonic contribution is more than an order of magnitude smaller. For sizable values of the EPC and at low temperature, the anharmonicity is negligible, showing that a measurement of the linewidth at $\mathbf{q}$ for the mode ν is essentially equivalent to determining $\lambda_{\mathbf{q}\nu}$. This is unexpected since earlier theoretical work [3,4,8] estimates anharmonicity to be important for a different but related quantity, the frequency shift.

Since the anharmonic contribution is negligible at Γ, A, and M, and computationally demanding, we evaluated only the EPC linewidth for the other points along the three directions. Using the calculated phonon frequencies, displacements, and linewidths, we compute the structure factors for one phonon process using the x-ray form factors, obtaining good agreement with experiment as shown in Figs. 1 and 2. In the top panel in Fig. 3 we show the theoretical results for the E_{2g} branch. The result is consistent with the experimental value wherever the E_{2g} branch is clearly visible, namely, along Γ-A and near the L point. Finally, the anharmonicity being negligible, we used Eq. (2) to extract $\lambda_{\mathbf{q}\nu}$ of the E_{2g} mode along Γ-A using the measured linewidths and frequencies together with the calculated electronic density of states. In Table II the experimental values are compared with the theoretical predictions. The anomalously large EPC along Γ-A is due to the nesting factor of the B bonding $p_{x,y}$ Fermi surfaces, which are concentric cylinders centered on Γ-A [5,6]. The E_{2g} modes, which modify the B-B distances, are the only ones with a sizable matrix element, $g^{\nu}_{\mathbf{k}n,\mathbf{k}+\mathbf{q}m}$, between electrons on these surfaces.

In conclusion, we have measured phonon dispersion and linewidths in a sub-mm-sized MgB_2 crystal with inelastic x-ray scattering, confirming the power and versatility of this technique. Both acoustic and optical modes are detected and we find that the E_{2g} mode is anomalously broadened along Γ-A but that this broadening is not generalized over the Brillouin zone. Our density functional theory calculations of the dispersion and linewidth are in excellent agreement with experiment. They show that the dominant contribution to the broadening for all modes is the electron-phonon coupling, the anharmonic contribution being much smaller. Thus, phonon linewidth in MgB_2 is a direct measure of electron-phonon coupling and could, with the availability of larger samples, be measured for all modes over the whole Brillouin zone so as to extract the anisotropic Eliashberg coupling function.

We acknowledge illuminating discussions with R. S. Gonnelli, P. Giannozzi, M. Xu, and F. Sette. The calculations were performed at the IDRIS supercomputing center. M. C. was supported by a Marie Curie Fellowship of the European Commission, Contract No. IHP-HPMF-CT-2001-01185.

[1] J. Nagamatsu *et al.*, Nature (London) **410**, 63 (2001).
[2] S. V. Shulga *et al.*, cond-mat/0103154.
[3] A. Y. Liu, I. I. Mazin, and J. Kortus, Phys. Rev. Lett. **87**, 087005 (2001).
[4] H. J. Choi *et al.*, Nature (London) **418**, 758 (2002); H. J. Choi *et al.*, Phys. Rev. B **66**, 020513 (2002).
[5] J. M. An and W. E. Pickett, Phys. Rev. Lett. **86**, 4366 (2001); J. M. An *et al.*, cond-mat/0207542.
[6] J. Kortus *et al.*, Phys. Rev. Lett. **86**, 4656 (2001).
[7] Y. Kong *et al.*, Phys. Rev. B **64**, 020501(R) (2001).
[8] T. Yildirim *et al.*, Phys. Rev. Lett. **87**, 037001 (2001).
[9] L. Boeri *et al.*, Phys. Rev. B **65**, 214501 (2002).
[10] K. Kunc *et al.*, J. Phys. Condens. Matter **13**, 9945 (2001).
[11] R. Osborn *et al.*, Phys. Rev. Lett. **87**, 017005 (2001).
[12] K. P. Bohnen, R. Heid, and B. Renker, Phys. Rev. Lett. **86**, 5771 (2001).
[13] A. F. Goncharov *et al.*, Phys. Rev. B **64**, 100509 (2001).
[14] P. Postorino *et al.*, Phys. Rev. B **65**, 020507(R) (2001).
[15] J. Hlinka *et al.*, Phys. Rev. B **64**, 140503(R) (2001).
[16] P. B. Allen, Phys. Rev. B **6**, 2577 (1972); P. B. Allen and R. Silberglitt, Phys. Rev. B **9**, 4733 (1974).
[17] J. Menéndez and M. Cardona, Phys. Rev. B **29**, 2051 (1984).
[18] G. Grimvall, *The Electron-Phonon Interaction in Metals* (North-Holland, Amsterdam, 1981), p. 201.
[19] T. Ruf *et al.*, Phys. Rev. Lett. **86**, 906 (2001).
[20] M. D'Astuto *et al.*, Phys. Rev. Lett. **88**, 167002 (2002).
[21] S. Baroni *et al.*, Rev. Mod. Phys. **73**, 515–562 (2001).
[22] J. P. Perdew, K. Burke, and M. Ernzerhof, Phys. Rev. Lett. **77**, 3865 (1996).
[23] N. Troullier and J. L. Martins, Phys. Rev. B **43**, 1993 (1991).
[24] S. G. Louie, S. Froyen, and M. L. Cohen, Phys. Rev. B **26**, 1738 (1982).
[25] P. Giannozzi *et al.*, Phys. Rev. B **43**, 7231 (1991).
[26] S. de Gironcoli, Phys. Rev. B **51**, 6773 (1995).
[27] A. Debernardi, S. Baroni, and E. Molinari, Phys. Rev. Lett. **75**, 1819 (1995).
[28] G. Lang *et al.*, Phys. Rev. B **59**, 6182 (1999).
[29] M. Lazzeri and S. de Gironcoli, Phys. Rev. B **65**, 245402 (2002). For the electronic BZ integration we used a $14 \times 14 \times 8$, $14 \times 14 \times 4$, and $7 \times 7 \times 8$ mesh for the calculation at Γ, A, and M, respectively. The third order derivatives of the total energy were computed with a $4 \times 4 \times 2$, $4 \times 4 \times 1$, and $2 \times 2 \times 2$ mesh of $\mathbf{q}$ points for Γ, A, and M, respectively and Fourier interpolated at the points $\mathbf{q}$ required for the BZ summation in Eq. (3). We performed the $\mathbf{q}$ BZ summation using a 20^3 grid of inequivalent points.